Intra-individual metameric variation expressed at the enamel-dentine junction of lower post-canine dentition of South African fossil hominins and modern humans

Lei Pan[1,2,*], John Francis Thackeray[3], Jean Dumoncel[2], Clément Zanolli[2], Anna Oettlé[4], Frikkie de Beer[5], Jakobus Hoffman[5], Benjamin Duployer[6], Christophe Tenailleau[6] and José Braga[2,3]

[1]Key Laboratory of Vertebrate Evolution and Human Origins of Chinese Academy of Sciences, Institute of Vertebrate Paleontology and Paleoanthropology, Chinese Academy of Sciences, Beijing 100044, China

[2]Laboratoire d'Anthropobiologie Moléculaire et d'Imagerie de Synthèse, UMR 5288 CNRS-Université de Toulouse (Paul Sabatier), Toulouse 31000, France

[3]Evolutionary Studies Institute and School of Geosciences, University of the Witwatersrand, PO WITS, Johannesburg 2050, South Africa

[4]Department of Anatomy, School of Medicine, Faculty of Health Sciences, University of Pretoria, Pretoria, South Africa

[5]Radiation Science Department, South African Nuclear Energy Corporation (Necsa), Pelindaba, North West Province, South Africa

[6]Centre Inter-universitaire de Recherche et d'Ingénierie des Matériaux, UMR 5085 CNRS-Université de Toulouse (Paul Sabatier), Toulouse Cedex 9, 31062, France

* Correspondence: Lei Pan, Key Laboratory of Vertebrate Evolution and Human Origins of Chinese Academy of Sciences, Institute of Vertebrate Paleontology and Paleoanthropology, Chinese Academy of Sciences, 142 Xizhimenwai Str. IVPP, 100044 Beijing, China. Email: panlei@ivpp.ac.cn

Abstract

Objectives

The aim of this study is to compare the degree and patterning of inter- and intra-individual metameric variation in South African australopiths, early *Homo* and modern humans. Metameric variation likely reflects developmental and taxonomical issues, and could also be used to infer ecological and functional adaptations. However, its patterning along the early hominin postcanine dentition, particularly among South African fossil hominins, remains unexplored.

Materials and Methods

Using microfocus X-ray computed tomography (μXCT) and geometric morphometric tools, we studied the enamel-dentine junction (EDJ) morphology and we investigated the intra-

and inter-individual EDJ metameric variation among eight australopiths and two early *Homo* specimens from South Africa, as well as 32 modern humans.

Results

Along post-canine dentition, shape changes between metameres represented by relative positions and height of dentine horns, outlines of the EDJ occlusal table are reported in modern and fossil taxa. Comparisons of EDJ mean shapes and multivariate analyses reveal substantial variation in the direction and magnitude of metameric shape changes among taxa, but some common trends can be found. In modern humans, both the direction and magnitude of metameric shape change show increased variability in M_2-M_3 compared to M_1-M_2. Fossil specimens are clustered together showing similar magnitudes of shape change. Along M_2-M_3, the lengths of their metameric vectors are not as variable as those of modern humans, but they display considerable variability in the direction of shape change.

Conclusion

The distalward increase of metameric variation along the modern human molar row is consistent with the odontogenetic models of molar row structure (inhibitory cascade model). Though much remains to be tested, the variable trends and magnitudes in metamerism in fossil hominins reported here, together with differences in the scale of shape change between modern humans and fossil hominins may provide valuable information regarding functional morphology and developmental processes in fossil species.

1 INTRODUCTION

In mammalian teeth, metameric variations observed among species may reflect differences in developmental processes (Braga, Thackeray, & Subsol, 2010; Evans, Daly, & Catlett, 2016; Morita, Morimoto, & Ohshima, 2016; Weiss, 1990). For instance, size-related shape variations in human upper molars are consistent with odontogenetic models of molar row structure and molar crown morphology (inhibitory cascade model) (Kavanagh, Evans, & Jernvall, 2007). Metameric variation could also be used to infer ecological conditions and/or functional adaptations (Kavanagh et al., 2007; Polly, 2007), as well as to distinguish symplesiomorphic traits from autamorphic traits (Hlusko, 2002). Dental metameric studies also yield some insights into primate taxonomy (e.g., Bailey, Benazzi, and Hublin, 2014, 2016; Braga et al., 2010; Hlusko, 2002; Morita et al., 2016; Singleton, Rosenberger, and Robinson, 2011; Weiss, 1990). However, few analyzes of metameric variation have yet been conducted at the intra-individual level (i.e., strictly based on teeth from the same individuals) (Braga et al., 2010): most studies were based on teeth representing different sets of individuals (Hlusko, 2002; Olejniczak, Gilbert, & Martin, 2007; Skinner, Gunz, & Wood, 2008a; Smith, Olejniczak, & Reid, 2006). Besides the potential usefulness of metameric variation for developmental, functional/ecological and taxonomic inferences, it may also help to identify position of isolated teeth among fossil hominin assemblages.

Previous studies of metameric variation mainly focused on the outer enamel surface (OES) (Hlusko, 2002; Singleton et al., 2011). Since the assessment of OES features may be obscured by occlusal wear, more recent analyses have investigated the enamel-dentine

junction (EDJ). However, only a few studies have yet dealt with the relevance of the EDJ morphology for assessing metameric variation in hominin teeth (Braga et al., 2010; Skinner et al., 2008a). As noted by Braga et al. (2010), modern humans exhibit stronger metameric variation between first and second molars, as compared with *Au. africanus*. Another study based on EDJ shape showed that *Au. africanus* and *P. robustus* display similar 3D-EDJ intra-taxon metameric trend along the molar dentition, but *P. robustus* preserves a marked reduction in the buccolingual breadth of the distal crown between M_2 and M_3, and a marked interradicular extension of the enamel cap in M_1 and M_2 (Skinner et al., 2008a).

Here we assess the metameric variation within and between individuals and groups at the EDJ along the post-canine dentition in three Plio-Pleistocene hominin taxa (*Australopithecus*, *Paranthropus* and early *Homo*) and in modern humans. We mainly aim to test whether the intra- and inter-individual metameric patterns and scales differ between australopiths and genus *Homo*. In other words, is the metameric variation observed in modern humans seen in early *Homo* and/or australopiths? We also test if 3D-EDJ metameric variation is a useful indicator of dental position in lower postcanine teeth.

2 MATERIALS AND METHODS

2.1 Study sample

We selected only the postcanine dentition from mandibular specimens—isolated teeth were excluded—to study the intra-individual metameric variation. Whenever the antimeres were preserved, only the teeth on the better preserved side were used in our analyses. The fossil hominin materials came from collections housed at the Ditsong Museum of Natural History (Pretoria, South Africa). Our fossil sample includes permanent lower post-canine teeth representing *P. robustus* ($N = 17$, six individuals), *Au. africanus* ($N = 4$, one individual) and early Pleistocene *Homo* specimens, attributed to *Homo erectus s.l.* (Wood, 2010; but see Clarke, 1985; Curnoe, 2006). The modern human reference material includes 88 teeth, representing 32 individuals of European, Asian and African origin (Table 1).

Because of unconformable wear stages in many modern specimens that affected the EDJ morphology in molar dentition, we used different individuals for comparisons M_1-M_2 and M_2-M_3 (detailed in Table 1). The degree of wear for each fossil specimen is listed in Table 1, according to tooth wear categories proposed by Molnar (1971). In the majority of cases, our specimens show no dentine horn wear on EDJs, but when necessary the dentine horn tip was reconstructed based on the morphology of the intact cusps.

The specimens were scanned using four comparable X-ray microtomographic instruments: an X-Tek (Metris) XT H225L industrial μXCT system at the South African Nuclear Energy Corporation (Necsa) (Hoffman & de Beer, 2012), a Scanco Medical X-Treme micro-XCT scanner at the Institute for Space Medicine and Physiology (MEDES) of Toulouse, a Phoenix Nanotom 180 scanner from the FERMAT Federation from the Inter-university Material Research and Engineering Centre (CIRIMAT, UMR 5085 CNRS), and a 225 kV-μXCT scanner housed at the Institute of Vertebrate Paleontology and Paleoanthropology (IVPP, Chinese Academy of Sciences). Isometric voxel size ranged from 10 to 70 μm. Each specimen was segmented in Avizo 8.0 (Visualization Sciences Group, www.vsg3d.com).

Micro-XCT image stacks were imported for semi-automated (modules "magic wand" and "threshold") and automated (module "watershed") segmentations. After the segmentation, the EDJ surface was generated using the "unconstrained smoothing" parameter.

Table 1. Composition of the study sample

| Specimen	P_3	P_4	M_1	M_2	M_3	Provenance	Age	Occlusal wear	Citations[a]
P. robustus									
SK 6	1	1	1	1	1	Mb. 1, HR **Swartkrans**	1.80 ± 0.09 Ma–2.19 ± 0.08 Ma (Gibbon et al., 2014), 2.31–1.64 Ma (Pickering et al., 2011)	1–3	1–2
SK 843			1		1	Mb. 1, HR		2–3	1
SK 61	1	1				Mb. 1, HR		1	3
SK 63	1	1	1	1		Mb. 1, HR		1	1
SKW 5			1		1	Mb. 1, HR		1–late 2	4
SKX 4446		1	1			Mb. 2	1.36 ± 0.69 Ma (Balter et al., 2008)	1–3	5
Au. africanus									
Sts 52	1	1		1	1	Mb. 4 **Sterkfontein**	3.0–2.5 Ma (White, Harris, 1977; Tobias, 1978; Clarke, 1994), 2.8–2.4 Ma (Vrba, 1985; but see Berger et al., 2002), 2.1 ± 0.5 Ma (Schwarcz et al., 1994)	2–3	1
Early *Homo*									
SKX 21204	1	1				Mb. 1, LB **Swartkrans**	1.80 ± 0.09 Ma–2.19 ± 0.08 Ma (Gibbon et al., 2014), 2.31–1.64 Ma (Pickering et al., 2011)	1	4
SK 15			1		1	Mb. 2	1.36 ± 0.69 Ma (Balter et al., 2008)	2–3	6
Extant *H. sapiens*	12	12	14	14/18[b]	18	South Africa/Europe/East Asia		1– late 2	7

[a] Citations: (1) Robinson (1956); (2) Broom (1949); (3) Broom and Robinson (1952); (4) Grine and Daeglin (1993); (5) Grine (1989); (6) Broom and Robinson (1949); (7) Rampont (1994).

[b] Owing to different wear stages, 32 M_2s were taken into account. 14 of them belong to the same individuals as M_1s, they were used in the analyses M_1-M_2. The other 18 teeth belong to the same individuals as M_3s, they were used in the analyses M_2-M_3.

2.2 Analyses

In some cases, especially in fossil specimens, only a tooth from one side is preserved (details in Table 1). Any image data from the left side were flipped to obtain a homogeneous right-

sided sample. For each tooth, we defined a set of main landmarks as well as a set of semi-landmarks along the marginal ridge between the main dentine horns (DHs), as an approximation of the marginal ridge (Figure 1). Along each semi-landmark section, a smooth curve was interpolated using a B-spline function using the "Create Splines" module. Interpolated curves were then imported into R (R Development Core Team, 2012), and were resampled to collect semi-landmarks that were equally spaced along each section/curve, delimited by traditional landmarks. For premolars, the main landmarks were placed on the tips of the DHs (i.e., 1. protoconid, 2. metaconid), with 55 semi-landmarks in between (15 on the mesial marginal ridge, 30 on the distal marginal ridge and 10 on the essential crest that connects the two DHs). The molar landmark set included four main landmarks on the tips of the DHs (i.e., 1. protoconid, 2. metaconid, 3. entoconid, 4. hypoconid), with 60 semi-landmarks, forming a continuous line, beginning at the tip of the protoconid and moving in a counter-clockwise direction.
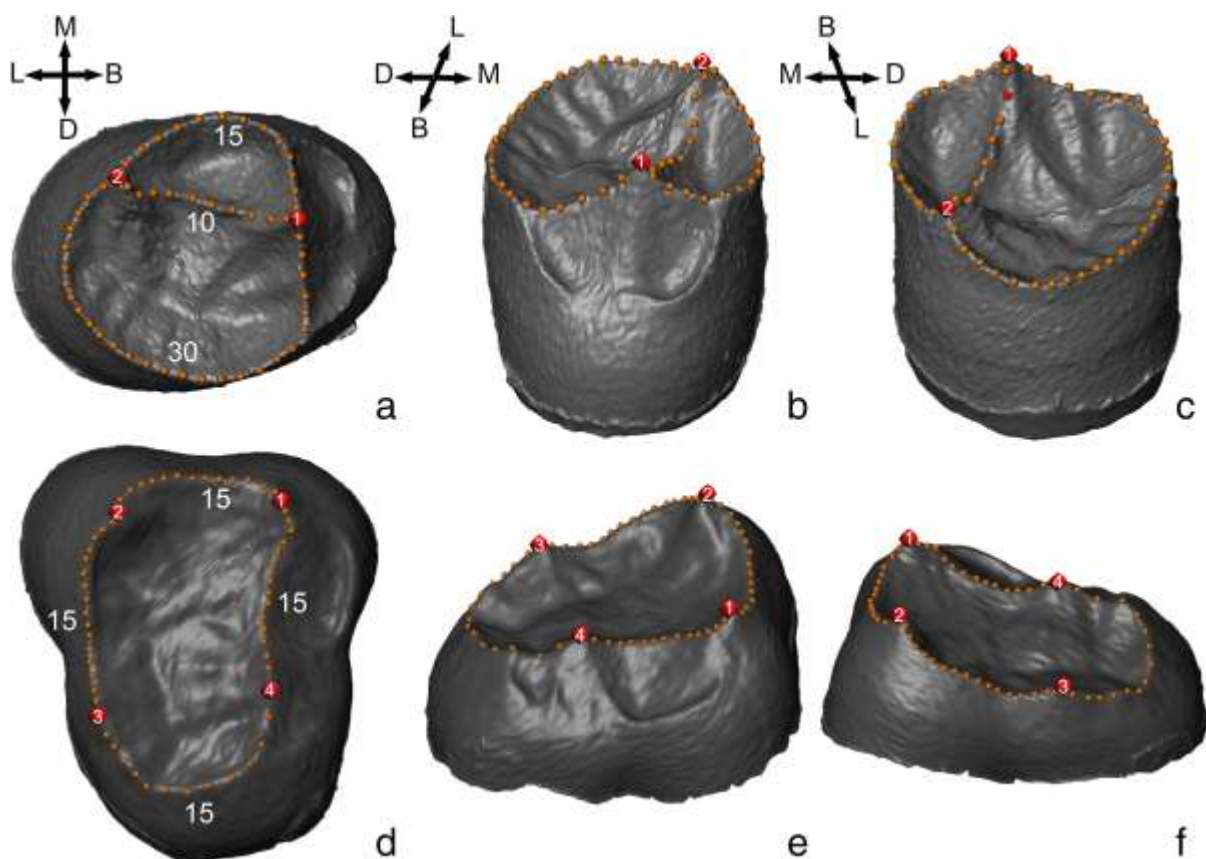
Figure 1. EDJ surface model of a lower premolar (A–C, SKX 21204 from Swartkrans) and a lower molar (D–F, SKW 5 from Swartkrans), illustrating the landmarks collected on the tips of the dentine horns (red spheres) and semi-landmarks that run between the dentine horns (orange spheres) used to capture EDJ shape. Abbreviations: buccal (B), distal (D), lingual (L) and mesial (M). Numbers on the red spheres stand for landmarks collected on the dentine horn tips, numbers next to the ridge curves stand for number of semi-landmarks. Note that relative sizes of premolars to molars are not to scale

In order to investigate intra-taxon metameric variation, the samples were grouped into three pairs, according to tooth position (P_3-P_4, M_1-M_2, M_2-M_3), and comparisons were performed within each pair.

The landmark sets were imported in R software (R Development Core Team, 2012), and statistical analyses were conducted subsequently. The study of intra-individual metameric variation in shape was completed using R packages ade4 and Morpho; each sample of landmark configurations was registered using generalized Procrustes analysis (GPA; Gower, 1975), treating semi-landmarks as equally spaced points. The resulting matrix of shape coordinates was analyzed in three ways. First, to visualize the average metameric shape differences for each taxon, mean configurations of each of the tooth classes (except for early *Homo* and *Au. africanus* represented by an isolated individual) were created, and superimposed using smooth curves with regard to tooth positons.

A between-group PCA (bgPCA) was performed based on the Procrustes shape coordinates to explore the distribution of each group in shape space (Braga, Thackeray, & Dumoncel, 2013; Gunz, Ramsier, & Kuhrig, 2012; Mitteroecker & Bookstein, 2011; Pan, Dumoncel, & de Beer, 2016; Ritzman, Terhune, & Gunz, 2016). The bgPCA computes a covariance matrix of the predefined group means and then projects all specimens into the space spanned by the eigenvectors of this covariance matrix. Between-group PCAs were conducted separately for each of the metameric pairs (P_3-P_4, M_1-M_2, M_2-M_3). Because early *Homo* and *Au. africanus* have only one specimen, respectively, representing their groups, they were projected subsequently onto the shape space, ordinated by the modern human and *P. robustus* tooth means, without being assigned to groups *a priori*. The first two axes were plotted in order to visualize the trends and vectors of EDJ shape change between metameres of the same individual. As the metameric vectors generated by bgPCA are actually placed in a multidimensional shape space, the bgPC1-bgPC3 axes were also plotted, shown in Supporting Information Figure S1. Our interpretation of the spatial positions and metameric vectors between specimens are mainly based on the first two bgPCs, but we refer to the third bgPC as well. As a complementary method of comparing the magnitude of shape variation between metameres, hierarchical clustering (HC) as well as subsequent dendrograms were computed. Dendrograms were obtained from the decomposition of the total variance (inertia) in between- and within-group variance. Contrary to the bgPCA, the HC does not require any *a priori* classification and specimens are aggregated into clusters according to the distances recorded between them. Aimed at finding how the metameric variation between fossils compares to modern human sample in the shape space, we used Euclidean distances between metameric pairs for clustering. We visualized the magnitude of shape variation using dendrograms and a 0 to 25 scale. Ward's minimum variance method was applied in HC, as it aims at finding compact clusters in which individuals are grouped. We chose to use this method because it minimizes the increase of intra-group inertia, and maximizes the inter-group inertia, at each step of the algorithm.

3 RESULTS

The within-taxon metameric variation of P_3-P_4, M_1-M_2 and M_2-M_3 mean shapes are illustrated in Figures 2 and 3; bgPCA plots and dendrograms are illustrated in Figure 4, and the bgPC1-bgPC3 axes are plotted in Supporting Information Figure S1, with the max-min values along the first two bgPC axes shown as landmark series in Supporting Information Figure S2. Specimens are marked according to species and dental position.
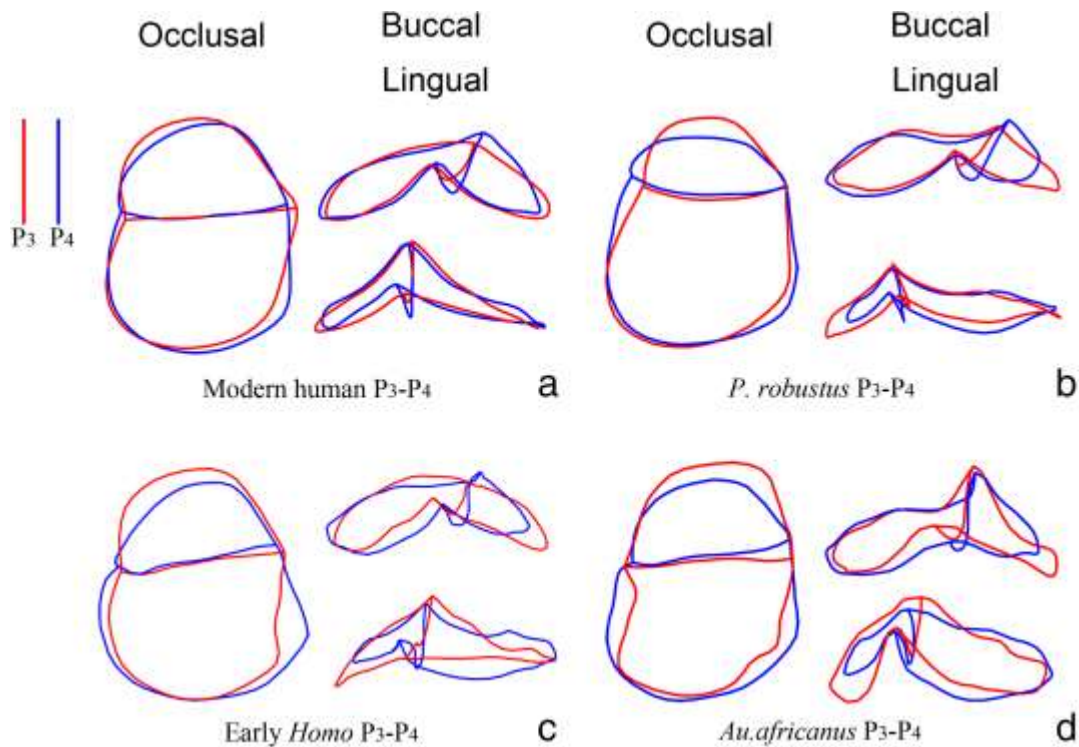
Figure 2. Comparison of metameric variation between P_3-P_4 based on mean shapes of the EDJ, after Procrustes superimposition. EDJ ridge curves are shown in occlusal, buccal and lingual views. Colors indicate different dental positions

Our analyses observed appreciable variation in the metameric relationships within and between taxa, but some common trends in shape change can be found. From P_3 to P_4, a distalward displacement of the mesial marginal ridge is shared among taxa (Figure 2); a decrease in the height of metaconid dentine horn is presented in modern humans, *P. robustus* and early *Homo* (Figure 2A–C); an increase in the height of protoconid dentine horn is seen in early *Homo* and *Au. africanus* (Figure 2C,D), a lingually placed metaconid dentine horn is seen in *P. robustus* (Figure 2B). Shape changes seen from the occlusal table (from a buccolingually elongated outline to a rounder outline) are shown in all four taxa, but are less expressed in modern humans compared to fossil groups. With regard to multivariate analyses, bgPC1 is mostly driven by the development of the anterior and posterior foveae, as well as by the height of dentine horns (Figure 4A; Supporting Information Figure S2A,B). BgPC2 is driven by the ratio between mesiodistal and buccolingual diameter, resulting in changes of EDJ outline (slender or oval) and metaconid dentine horn height (Figure. 4A; Supporting Information Figure S2C,D). Metameric vectors plotted using the first two bgPCs show that, in *P. robustus* and modern humans, although within-taxon differences can be seen, the trends of shape change are similar for both taxa (except for two modern human individuals), which is consistent with results seen in mean shape superimposition (Figure 2A,B). But along bgPC3 axis, modern humans display a more variable trend of shape change compared with *P. robustus* (Supporting Information Figure S1A). *P. robustus* specimen SK 6 shows a considerable magnitude of shape change along bgPC2 and bgPC3 axes, increasing the within-group metameric variation (Figure 4A, Supporting Information Figure S1A). With regard to the early *Homo* individual SKX 21204, the direction of its metameric vector shows a somewhat close affinity to that of the *Au. africanus* specimen Sts 52 (Figure 4A, Supporting Information Figure S1A). In the axes

represented here, the shapes of their P_3s resemble those of modern humans (note that Sts 52 P_3 is placed just between the range of modern humans and *P. robustus*), but their P_4s are similar to those of *P. robustus* (Figure 4A, Supporting Information Figure S1A). But as our analyses mixed interspecific and metameric variation, inferences of EDJ shape differences/similarities between isolated cases should be carefully addressed.
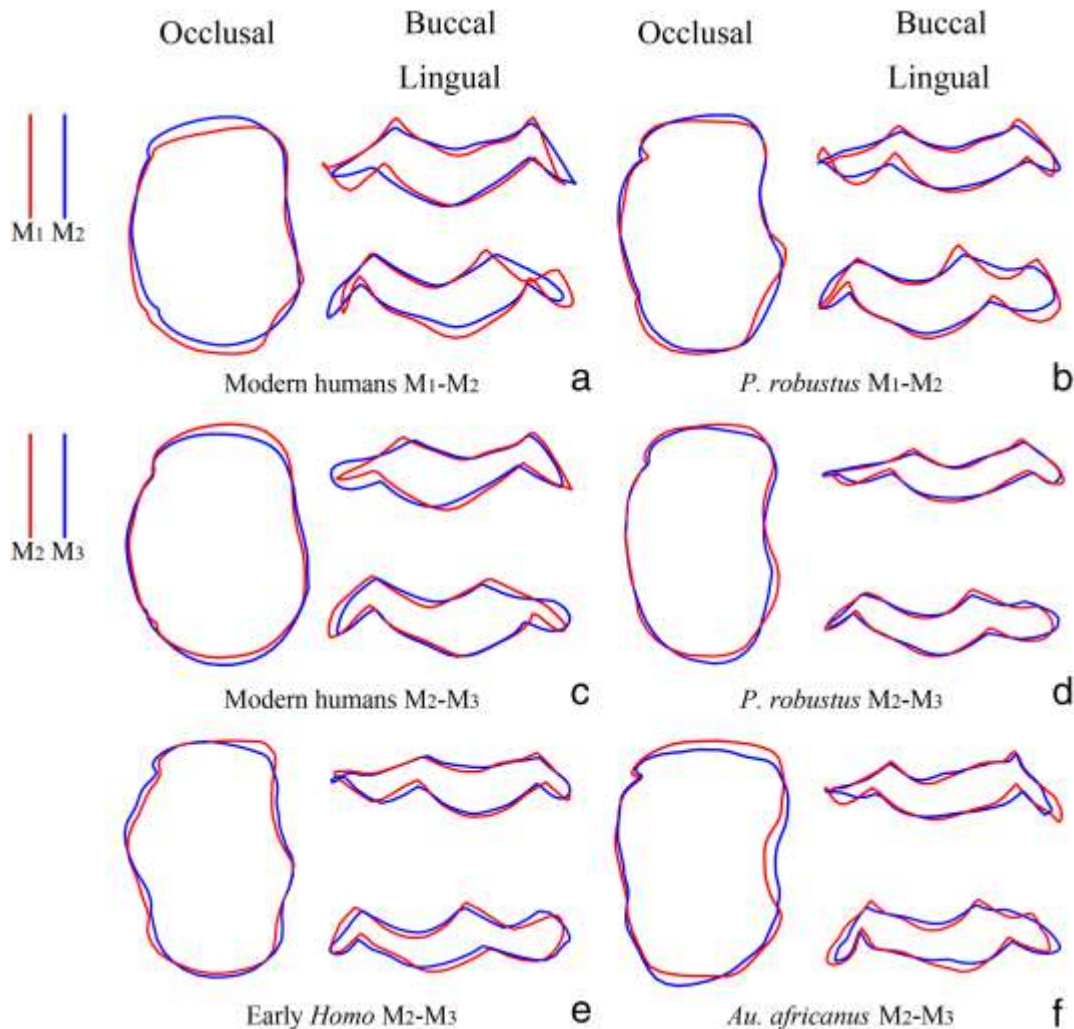

Figure 3. Comparison of metameric variation between M_1-M_2, and between M_2-M_3, based on mean shapes of the EDJ, after Procrustes superimposition. EDJ ridge curves are shown in occlusal, buccal and lingual views. Colors indicate different dental positions. A–B: M_1 (red) compared to M_2 (blue); C–F: M_2 (red) compared to M_3 (blue)

Almost all modern human M_2s and many M_3s lack a hypoconulid, and hence hypoconulid dentine horn tip was not included in the homologous landmarks (Figure 1D–F). Therefore, differences in the hypoconulid dentine horn height and relative position are not recorded in the present study. In metameres M_1-M_2, there is a marked reduction in the height of dentine horns of both *P. robustus* and modern humans, particularly in the talonid, resulting in a flattened topology in M_2 (Figure 3A,B); entoconid dentine horn is more centrally placed in M_2 (a pattern that is more marked in modern humans). Unfortunaltely, materials from early *Homo* and *Au. africanus* are not avaliable for comparison. With regard to multivariate analyses, similar magnitude of shape change is seen in both species (Figure 4B,E; Supporting Information Figure S1B). The bgPC1 axis is driven by the presence of the hypoconulid, and

the position and height of the hypoconid dentine horn; while the bgPC2 axis is driven by the height of the lingual dentine horns (Figure 4B; Supporting Information Figure S2E–H). It is worth noticing that SK 6 M_1-M_2 show a unique trend of shape change along the bgPC1, and SK 63 has a much shorter metameric vector in bgPC1-bgPC2 plot, increasing the within-group metameric variation in *P. robustus*. In shape space bgPC1-bgPC3, *P. robustus* shows vertically-oriented metameric vectors with similar lengths contrasted with modern humans; along bgPC3, the direction of shape change in modern humans is more variable compared to bgPC1 (Supporting Information Figure S1B). Our results of hierachichal clustering reveal that, although placed separately from modern groups, the *P. robustus* sample displays closer affinity to a few modern individuals, indicating a similarity in intra-individual metameric distances (Figure 4E).

For metameres M_2-M_3, a slight distal expansion of the marginal ridges is observed except for the early *Homo* specimen, SK 15 (Figure 3C–F). A reduction in the height of dentine horns on the talonid is seen in modern humans and australopiths (a pattern that is more marked in modern humans; Figure 3C,D). Changes in the relative positions of the dentine horns are widely observed: for modern humans, talonid dentine horns are more centrally placed in M_2 than in M_3 (Figure 3C; buccal view); for australopiths, the hypoconid dentine horn is more centrally placed in M_3, more markedly in *P. robustus*, in addition, *Au. africanus* individual displays a more centrally placed entoconid in M_2 (Figure 3D,F; occlusal view); for the early *Homo* specimen SK 15, a more centrally placed protoconid and entoconid dentine horns are seen in M_3 (Figure 3E; occlusal view). With regard to multivariate analyzes, the bgPC1 exhibits shape changes in the EDJ outline (oviod to elongated, Supporting Information Figure S2I,J) and changes in the height of the distal dentine horns (low to high, Supporting Information Figure S2I,J). Our bgPCA reveals similar directions of metameric vectors between modern humans and Sts 52, the *Au. africanus* specimen (except for two modern human individuals). But in the shape space defined by bgPC1-bgPC3 (Supporting Information Figure S1C), the direction and length of metameric vector of Sts 52 are similar to *P. robustus* specimen, SK 843. In fact, all the fossil specimens show somewhat vertically-oriented metameric vectors, a pattern which is only observed in two of the modern human specimens (Supporting Information Figure S1C). Moreover, in fossils an appreciable scale of within-individual shape change is found along bgPC3 axis, among which SK 15 shows the shortest metameric vector. Despite the fact that fossil specimens display closer magnitude of shape change (Figure 4D–F), it is found that the directions of metameric shape change among fossil groups/individuals are quite diversified (Figures 3C–F and 4C; Supporting Information Figure S1C). Represented by the first three bgPCs, modern humans show considerable diversification in the length and direction of metameric vectors. It is also worth nothing that, in the three axes shown here, modern human M_3s show a much wider shape variability than M_2s.
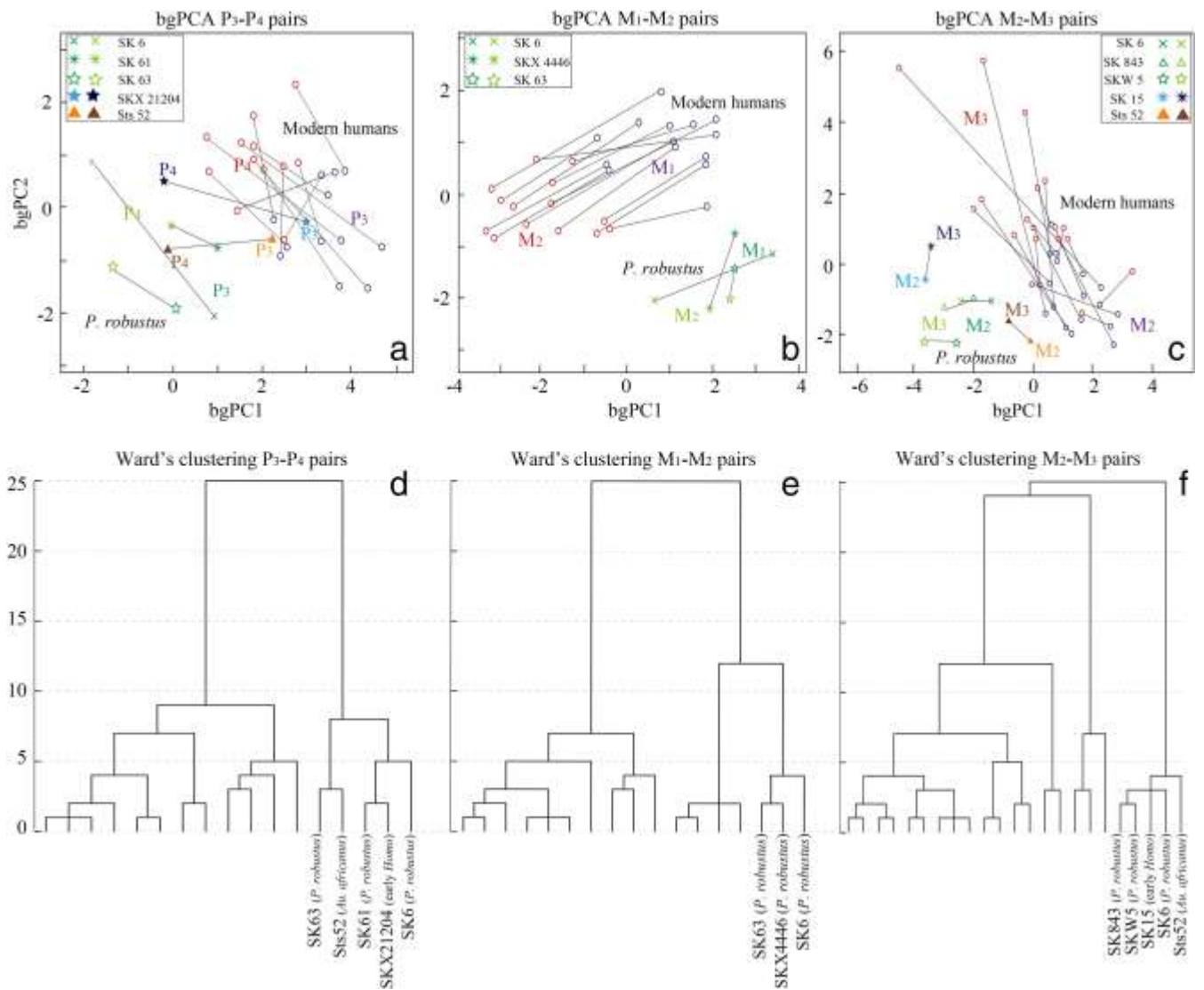
Figure 4. A–C: Results of bgPCA of the semi-landmark configurations. Axes represent functions of the shape variation, specimens from the same individual are marked using the same symbol (for easier visual inspection, all of the modern individuals are marked using the same symbol), and each color representing the tooth position for each taxon. Metameres are connected using lines, showing metameric vectors. D–F: Dendrograms of intra-individual metameric variation in EDJ shape yielded by Hierachical Clustering (HC), showing the magnitude of metameric variation within and between groups. HC was done between metameric pairs P_3-P_4 (D), M_1-M_2 (E), and M_2-M_3 (F). Scales from 0 to 25 indicate similitude of metameric shape variation between individuals. For easier visual inspection, only fossil specimens are marked

4 DISCUSSION

Tooth morphology is controlled by the combined effects of biochemical signaling degraded from mesial to distal direction at the tooth row level and at the individual crown level (Jernvall, 2000; Weiss, 1990). As suggested by the inhibitory cascade model (Evans et al., 2016; Kavanagh et al., 2007), the development of each deciduous and permanent molar is controlled by the balance between inhibitor molecules from mesially located tooth germs and activator molecules from the mesenchyme. The ratio of genetic activation and

inhibition during development determines the relative size of the dental elements in the dental row. However, permanent premolars are derived independently from deciduous molars, so the tooth germs of P_3 and P_4 are not directly connected, therefore caution should be addressed when linking inhibitory cascade model to the metameric variation in permanent premolars.

Metameric differences are often subtle, and the risk of conflating metameric and taxonomic variation is a general concern (Hlusko, 2002; Singleton et al., 2011). However, dental metameric variation in Plio-Pleistocene hominins remains relatively unexplored owing to difficulty in quantifying the complex and subtle shape variation in premolar and molar crowns, especially at the level of the EDJ. By investigating the dental inner structure, we report distinctive features with regard to EDJ shapes of the lower post-canine dentition in fossil taxa, but fossil and modern groups share some intra-individual metameric patterns.

Using geometric morphometric tools, we first document the intra-individual metameric shape changes in premolars of modern human, *P. robustus* and one early *Homo* specimen. Based on the mean-shape superimposition, our modern humans and *P. robustus* show similar changes in the height of dentine horns from P_3 to P_4, whereas this change is not found in *Au. africanus*. The early *Homo* premolar row displays an intermediate condition between modern humans/*P. robustus* and *Au. africanus* with regard to the changes in the dentine horn height. But due to the small sample size, further investigation will be needed. In all three pairs of metameres, hierarchical clustering placed fossil specimens together, showing similar degree of shape change, but the magnitude of metameric variation is quite diversified in modern humans. Moreover, as revealed by our bivariate plots, modern human M_3s show a large scale of shape variability. This is consistent with previous observations using conventional tools (Garn, Lewis, & Kerewsky, 1963; Townsend, Richards, & Hughes, 2003) or geometric morphometrics (Morita et al., 2016; Pan et al., 2016). It has been suggested that in modern humans, the inter-individual differences are larger for the M_2s than for the M_1s (Braga et al., 2010). This observation is in line with the distalward molar size reduction seen in Pleistocene humans (Bermúdez de Castro & Nicolas, 1995; Brace & Mahler, 1971; Brace, Rosenberg, & Hunt, 1987; Evans et al., 2016). Since the shape stability was considered to increase from third molar to first molar (Dahlberg, 1945), it is possible that small molar size results in a more unstable shape rather than larger molar size. Just as Skinner et al. (2008a) observed a small-scale, distal expansion of the marginal ridge in M_2-M_3s of *P. robustus*, we confirm such trend in all of our *P. robustus* specimens and in a number of modern humans. This trend is weakly expressed in our *Au. africanus* and is not presented in the early *Homo* specimen. A previous study observed that, in australopiths there is an increase in the height of mesial dentine horns from M_2 to M_3 (Skinner et al., 2008a), in contrast, we found a reduction in relative dentine horn height from M_1 to M_2, and from M_2 to M_3 among all the taxa examined here, similar to metameric patterns expressed in *Pan* (Skinner, Gunz, & Wood, 2009). We suggest that this is probably because of our small sample size, and the fact that our study is focused on intra-individual variation therefore only metameres from strictly the same individual were investigated. The early *Homo* dentition SK 15 displays similar degree of metameric variation to other fossil samples, closer to the three *P. robustus* specimens than to the *Au. africanus* specimen. In all, the three fossil groups display variable directions in the shape change. In modern humans, the direction and magnitude of metameric vectors show increased variability in metameres M_2-M_3, than in

M_1-M_2. However, in *P. robustus*, the length and direction of metameric vectors seem more variable in M_1-M_2 pairs, than in M_2-M_3 pairs, which show consistent metameric shape change. Further studies including more fossil specimens will be necessary to ascertain whether the metameric patterns observed here are characteristic of these groups.

5 CONCLUSIONS

While 2D studies based on the OES suggest the existence of a distinctive metameric pattern in modern humans compared with that found in chimpanzees and *Au. africanus* (Hlusko, 2002), in each comparative pair of EDJ (P_3-P_4, M_1-M_2 and M_2-M_3) that we investigated, we do not observe a specific metameric pattern that belongs only to extant humans, but rather a few common trends shared by groups despite a degree of inter- and intra-group variaiton. As a whole, the EDJ proves to be a reliable proxy to identify the taxonomic identity (Pan et al., 2016; Skinner et al., 2008a, 2008b, 2009b, 2016; Zanolli, 2015; Zanolli, Bondioli, & Mancini, 2012), but further research is needed to determine whether the metameric trends in 3D-EDJ observed here could act as one piece of evidence to identify tooth position from isolated specimens. Moreover, the underlying mechanisms remain to be answered. Along the molar dentition, based on the axes examined in this study, our results with regard to modern humans are generally in accordance with morphogenetic models of molar rows and molar crowns (inhibitory cascade model). In *P. robustus* specimens examined here, trends of mean-shape changes from M_1 to M_2 and from M_2 to M_3 differed from each other, instead of a simple gradation, such differential expression of metamerism has been previously reported in modern human upper molars (Morita et al., 2016). It should be noted that our study focuses only on the EDJ marginal ridges, but additional studies of the accessory ridges (e.g. protostylid), and a more global analysis of shape variation among early hominins based on the whole EDJ surface and diffeomorphisms (Braga, 2016) will supplement our understanding on the metameric variation in hominin dentition.

References

Bailey, S. E., Benazzi, S., Buti, L., & Hublin, J. J. (2016). Allometry, merism, and tooth shape of the lower second deciduous molar and first permanent molar. *American Journal of Physical Anthropology,* 159, 93–105.

Bailey, S. E., Benazzi, S., & Hublin, J. J. (2014). Allometry, merism, and tooth shape of the upper deciduous M2 and permanent M1*. American Journal of Physical Anthropology,* 154, 104–114.

Balter, V., Blichert-Toftv, J., Braga, J., Telouk, P., Francis, T., & Albarède, F. (2008). U-Pb dating of fossil enamel from the Swartkrans Pleistocene hominid site, South Africa. *Earth and Planetary Science Letters,* 267, 236–246.

Berger, L. R., Lacruz, R., & de Ruiter, D. J. (2002). Revised age estimates of Australopithecus-bearing deposits at Sterkfontein*, South Africa. American Journal of Physical Anthropology,* 119, 192–197.

Bermúdez de Castro, J. M., & Nicolas, M. E. (1995). Posterior dental size reduction in hominids: The Atapuerca evidence. *American Journal of Physical Anthropology,* 96, 335–356.

Brace, C. L., & Mahler, P. E. (1971). Post-Pleistocene changes in the human dentition. *American Journal of Physical Anthropology*, 34, 191–203.

Brace, C. L., Rosenberg, K. R., & Hunt, K. D. (1987). Gradual change in human tooth size in the late Pleistocene and post-Pleistocene*. Evolution,* 41, 705–720.

Braga, J. (2016). In press. The Kromdraai hominins revisited with an updated portray of differences between Australopithecus africanus and Paranthropus robustus. In J. Braga & F. Thackeray (Eds.), *Kromdraai, a birthplace of Paranthropus in the Cradle of Humankind.* Johannesburg: Sun Media Metro.

Braga, J., Thackeray, J. F., Dumoncel, J., & Fourvel, J.-B. (2013). A new partial temporal bone of a juvenile hominin from the site of Kromdraai B (South Africa). *Journal of Human Evolution,* 65, 447–456.

Braga, J., Thackeray, J. F., Subsol, G., Kahn, J. L., Maret, D., Treil, J., & Beck, A. (2010). The enamel-dentine junction in the postcanine dentition of Australopithecus africanus: Intra-individual metameric and antimeric variation. *Journal of Anatomy,* 216, 62–79.

Broom, R. (1949). Another new type of fossil ape-man. *Nature,* 163, 57.

Broom, R., & Robinson, J. T. (1952). Swartkrans ape-man, *Paranthropus crassidens. Transvaal Museum Memoirs,* 6, 1–124.

Clarke, R. (1985). *Australopithecus* and early *Homo* in Southern Africa. In E. Delson (Ed.), *Ancestors: The hard* evidence (pp. 171–177). New York: Alan R. Liss.

Clarke, R. (1994). On some new interpretations of Sterkfontein stratigraphy. *South African Journal of Science,* 90, 211–214.

Curnoe, D. (2006). Odontometric systematic assessment of the Swartkrans SK 15 mandible. *Homo,* 57, 263–294.

Dahlberg, A. A. (1945). The changing dentition of man. *The Journal of the American Dental Association,* 32, 676–690.

Evans, A. R., Daly, E. S., Catlett, K. K., Paul, K. S., King, S. J., Skinner, M. M., … Jernvall, J. (2016). A simple rule governs the evolution and development of hominin tooth size. *Nature,* 530, 477–480.

Garn, S. M., Lewis, A. B., & Kerewsky, R. S. (1963). Third molar agenesis and size reduction of the remaining teeth. *Nature,* 200, 488–489.

Gibbon, R. J., Pickering, T. R., Sutton, M. B., Heaton, J. L., Kuman, K., Clarke, R. J., … Granger, D. E. (2014). Cosmogenic nuclide burial dating of hominin-bearing Pleistocene cave deposits at Swartkrans, South Africa. *Quaternary Geochronology,* 24, 10–15.

Gower, J. C. (1975). Generalized procrustes analysis. *Psychometrika,* 40, 33–51.

Grine, F. E. (1989). New hominid fossils from the Swartkrans formation (1979–1986 excavations): craniodental specimens. *American Journal of Physical Anthropology,* 79, 409–449.

Gunz, P., Ramsier, M., Kuhrig, M., Hublin, J. J., & Spoor, F. (2012). The mammalian bony labyrinth reconsidered, introducing a comprehensive geometric morphometric approach. *Journal of Anatomy,* 220, 529–543.

Hlusko, L. (2002). Identifying metameric variation in extant hominoid and fossil hominid mandibular molars. *American Journal of Physical Anthropology, 118, 86–97.*

Hoffman, J. W., & de Beer, F. (2012). Characteristics of the micro-focus X-ray tomography facility (MIXRAD) at Necsa in South Africa. 18th World Conference on Nondestructive Testing, Durban, South Africa.

Jernvall, J. (2000). Linking development with generation of novelty in mammalian teeth. *Proceedings of the National Academy of Sciences,* 97, 2641–2645.

Kavanagh, K. D., Evans, A. R., & Jernvall, J. (2007). Predicting evolutionary patterns of mammalian teeth from development. *Nature,* 449, 427–432.

Mitteroecker, P., & Bookstein, F. (2011). Linear discrimination, ordination, and the visualization of selection gradients in modern morphometrics. *Evolutionary Biology,* 38, 100–114.

Molnar, S. (1971). Human tooth wear, tooth function and cultural variability. *American Journal of Physical Anthropology,* 34, 175–189.

Morita, W., Morimoto, N., & Ohshima, H. (2016). Exploring metameric variation in human molars: A morphological study using morphometric mapping. *Journal of Anatomy,* 229, 343–355.

Olejniczak, A., Gilbert, C., Martin, L., Smith, T. M., Ulhaas, L., & Grine, F. E. (2007). Morphology of the enamel-dentine junction in sections of anthropoid primate maxillary molars. *Journal of Human Evolution,* 53, 292–301.

Pan, L., Dumoncel, J., de Beer, F., Hoffman, J., Thackeray, J. F., Duployer, B., … Braga, J. (2016). Further morphological evidence on South African earliest Homo lower postcanine dentition: Enamel thickness and enamel dentine junction. *Journal of Human Evolution,* 96, 82–96.

Pickering, R., Kramers, J. D., Hancox, P. J., de Ruiter, D. J., & Woodhead, J. D. (2011). Contemporary flowstone development links early hominin bearing cave deposits in South Africa. *Earth and Planetary Science Letters,* 306, 23–32.

Polly, P. D. (2007). Development with a bite. *Nature, 449,* 413–415.

R Development Core Team. (2012). R: A language and environment for statistical computing. Vienna: R Foundation for Statistical Computing.

Rampont, M. (1994). *Les Squelettes, os et Dents de Foetus, Nouveaux-Nés et Enfants du Musée Anatomique de Strasbourg: Aspects historiques et catalogue.* Louis Pasteur University.

Ritzman, T. B., Terhune, C. E., Gunz, P., & Robinson, C. A. (2016). Mandibular ramus shape of Australopithecus sediba suggests a single variable species. *Journal of Human Evolution,* 100, 54–64.

Robinson, J. T. (1956). The dentition of the Australopithecinae. *Transvaal Museum Memoirs,* 9, 1–179.

Schwarcz, H. P., Grün, R., & Tobias, P. V. (1994). ESR dating studies of the australopithecine site of Sterkfontein, South Africa. *Journal of Human Evolution,* 26, 175–181.

Singleton, M., Rosenberger, A. L., Robinson, C., & Oneill, R. (2011). Allometric and metameric shape variation in Pan mandibular molars: A digital morphometric analysis. *Anat Rec,* 294, 322–334.

Skinner, M. M., de Vries, D., Gunz, P., Kupczik, K., Klassen, R. P., Hublin, J. J., & Roksandic, M. (2016). A dental perspective on the taxonomic affinity of the Balanica mandible (BH-1). *Journal of Human Evolution,* 93, 63–81.

Skinner, M. M., Gunz, P., Wood, B. A., Boesch, C., & Hublin, J. J. (2008a). Enamel-dentine junction (EDJ) morphology distinguishes the lower molars of *Australopithecus africanus* and *Paranthropus robustus. Journal of Human Evolution,* 55, 979–988.

Skinner, M. M., Wood, B. A., Boesch, C., Olejniczak, A. J., Rosas, A., Smith, T. M., & Hublin, J.-J. (2008b). Dental trait expression at the enamel-dentine junction of lower molars in extant and fossil hominoids. *Journal of Human Evolution,* 54, 173–186.

Skinner, M. M., Gunz, P., Wood, B. A., Boesch, C., & Hublin, J. J. (2009). Discrimination of extant Pan species and subspecies using the enamel–dentine junction morphology of lower molars. *American Journal of Physical Anthropology,* 140, 234–243.

Smith, T. M., Olejniczak, A. J., Reid, D. J., Ferrell, R.J., & Hublin, J. J. (2006). Modern human molar enamel thickness and enamel–dentine junction shape. *Archives of Oral Biology,* 51, 974–995.

Tobias, P. V. (1978). The earliest Transvaal members of the genus Homo with another look at some problems of hominid taxonomy and systematics. *Zeitschrift für Morphologie und Anthropologie,* 69, 225–265.

Townsend, G., Richards, L., & Hughes, T. (2003). Molar intercuspal dimensions: Genetic input to phenotypic variation. *Journal of Dental Research,* 82, 350–355.

Vrba, E. S. (1985). Early hominids in southern Africa: updated observations on chronological and ecological background. In P. V. Tobias (Ed.), *Hominid evolution: Past, present and future* (pp 195–200). New York: Alan R. Liss.

Weiss, K. M. (1990). Duplication with variation: Metameric logic in evolution from genes to morphology*. Yearbook of Physical Anthropology,* 11, 1–23.

White, T. D., & Harris, J. M. (1977). Suid evolution and correlation of African hominid localities. *Science,* 198, 13–21.

Wood, B. (2010). Reconstructing human evolution: Achievements, challenges, and opportunities. *Proceedings of the National Academy of Sciences,* 107, 8902–8909.

Zanolli, C. (2015). Brief communication: Molar crown inner structural organization in Javanese Homo erectus. *American Journal of Physical Anthropology,* 156, 148–157.

Zanolli, C., Bondioli, L., Mancini, L., Mazurier, A., Widianto, H., & Macchiarelli, R. (2012). Brief communication: Two human fossil deciduous molars from the Sangiran Dome (Java, Indonesia): Outer and inner morphology. *American Journal of Physical Anthropology, 147, 472–481.*

Supporting Information
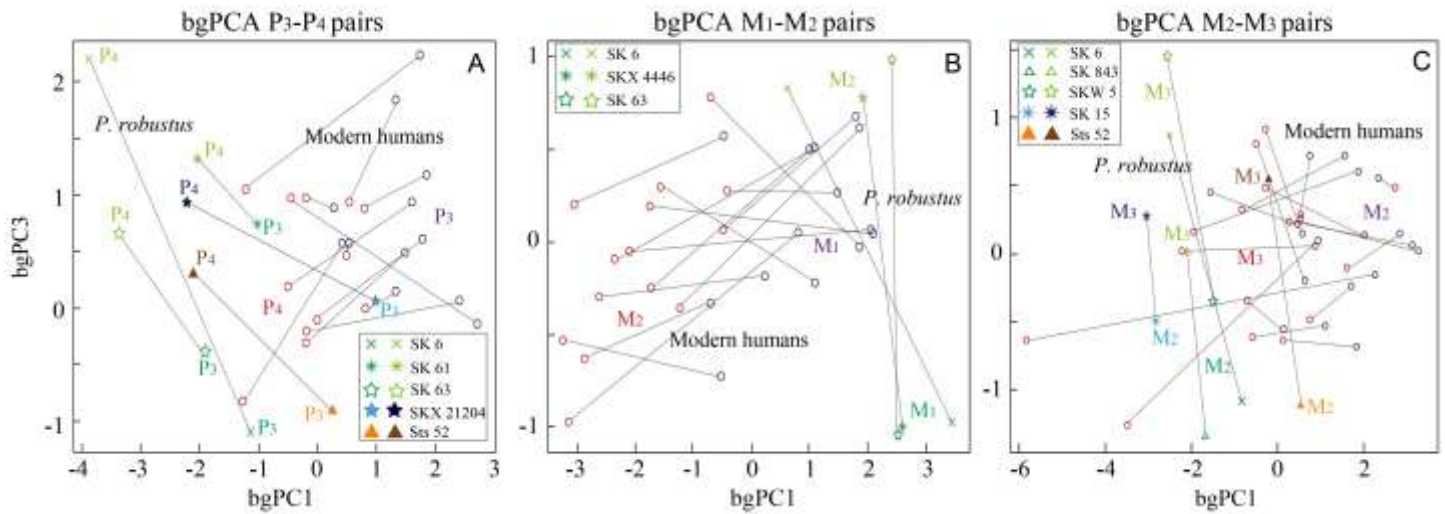
SOM Figure 1. Results of bgPCA of the semi-landmark configurations, showing bgPC1 and bgPC3. Axes represent functions of the shape variation, specimens from the same individual are marked using the same symbol (for easier visual inspection, all of the modern individuals are marked using the same symbol) and are connected using lines. Each color representing the tooth position for each taxon.
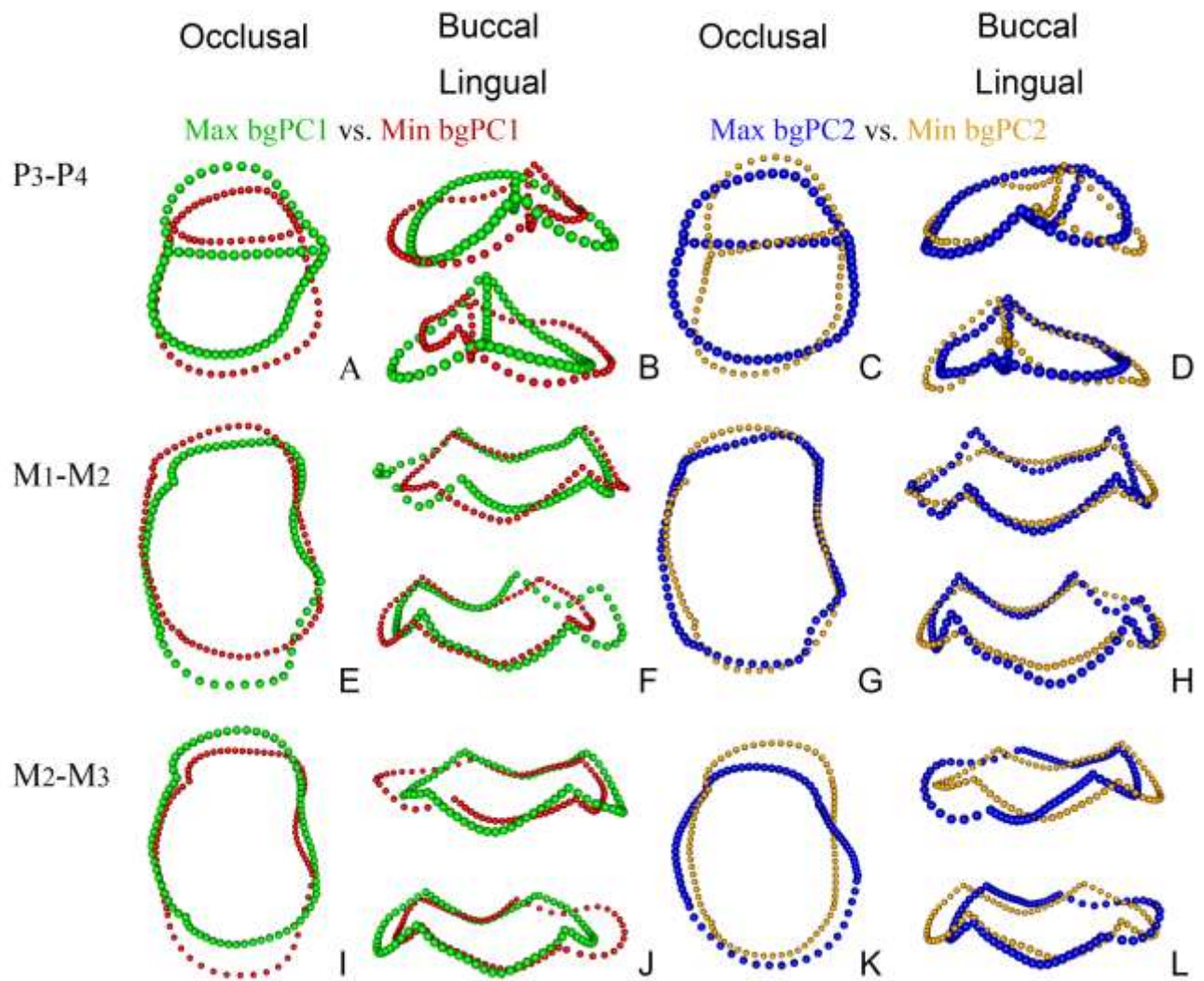
SOM Figure 2. Landmark series of EDJ after Procrustes superimposition and bgPCA, superimposed EDJ shapes are max-min values along the first two bgPC axes.